5-Year Associations among Cerebral Arterial Pulsatility, Perivascular Space Dilation, and White Matter Lesions

Tomas Vikner, MSc [ID],[1] Nina Karalija, PhD [ID],[1,2] Anders Eklund, PhD,[1,2] Jan Malm, MD, PhD,[3] Anders Lundquist, PhD,[2,4] Nikodemus Gallewicz, MD,[1] Magnus Dahlin, MD,[1] Ulman Lindenberger, PhD,[5,6,7] Katrine Riklund, MD, PhD,[1,2] Lars Bäckman, PhD,[8] Lars Nyberg, PhD,[1,2,9] and Anders Wåhlin, PhD[1,2,10]

Objective: High cerebral arterial pulsatility index (PI), white matter lesions (WMLs), enlarged perivascular spaces (PVSs), and lacunar infarcts are common findings in the elderly population, and considered indicators of small vessel disease (SVD). Here, we investigate the potential temporal ordering among these variables, with emphasis on determining whether high PI is an early or delayed manifestation of SVD.

Methods: In a population-based cohort, 4D flow MRI data for cerebral arterial pulsatility was collected for 159 participants at baseline (age 64–68), and for 122 participants at follow-up 5 years later. Structural MRI was used for WML and PVS segmentation, and lacune identification. Linear mixed-effects (LME) models were used to model longitudinal changes testing for pairwise associations, and latent change score (LCS) models to model multiple relationships among variables simultaneously.

Results: Longitudinal 5-year increases were found for WML, PVS, and PI. Cerebral arterial PI at baseline did not predict changes in WML or PVS volume. However, WML and PVS volume at baseline predicted 5-year increases in PI. This was shown for PI increases in relation to baseline WML and PVS volumes using LME models ($R \geq 0.24$; $p < 0.02$ and $R \geq 0.23$; $p < 0.03$, respectively) and LCS models ($\beta = 0.28$; $p = 0.015$ and $\beta = 0.28$; $p = 0.009$, respectively). Lacunes at baseline were unrelated to PI.

Interpretation: In healthy older adults, indicators of SVD are related in a lead–lag fashion, in which the expression of WML and PVS precedes increases in cerebral arterial PI. Hence, we propose that elevated PI is a relatively late manifestation, rather than a risk factor, for cerebral SVD.

ANN NEUROL 2022;92:871–881

Introduction

Cerebral small vessel disease (SVD) is characterized by dysfunction in cerebral arterioles, capillaries, and venules.[1] SVD is estimated to contribute to cognitive decline in approximately half of dementia cases, but its pathophysiology is poorly understood.[1, 2] Magnetic resonance imaging (MRI) features attributed to SVD include white matter lesions (WML), dilated perivascular spaces (PVSs), lacunar infarcts, microinfarcts, and microbleeds.[1, 3] These imaging biomarkers are widely present in the population, where they develop

with aging and the accumulation of vascular risk factors.[2, 4] Recently, the cerebral arterial pulsatility index (PI), a measure sensitive to large-artery stiffness and downstream microvascular resistance, has also been suggested as a potential biomarker that reflects early alterations in SVD.[1, 5]

Observing whether elevated cerebral arterial pulsatility is an *early* or *delayed* manifestation of SVD is necessary to inform models on SVD pathophysiology. One potential chain of events is that age-related arterial stiffness, with concomitant increases in arterial pulsatility, may lead to cerebral microvascular damage.[6] In animal[7] and *in vitro*[8] studies, excessive pulsatility is followed by endothelial dysfunction and blood–brain barrier (BBB) breakdown, which could contribute to SVD[1]. Alternatively, relationships between microvascular damage and pulsatility may be reciprocal. SVD is characterized by stiffening, increased tortuosity, and narrowing of the lumen of vessels[1] – factors that in turn could increase microvascular resistance and elevate arterial PI. Hence, increased PI is potentially a late manifestation of SVD.

Longitudinal examinations of these issues are limited to transcranial ultrasound studies and investigations of whether baseline pulsatility predicts changes in WML volume.[9, 10] Hence, previous studies have not examined the possibility that PVS and WML progression could co-occur with, or precede, increases in cerebral arterial pulsatility. The technique 4D flow MRI offers time-resolved 3D velocity encoding and angiographic imaging of the whole brain in a single scan.[11, 12] Semi-automatic post-processing methods using centerline processing schemes[13, 14] have made 4D flow feasible for investigating arterial stiffness and pulsatility in major[15, 16] as well as small cerebral arteries.[17, 18] By using such post-processing, age-sensitive metrics of pulsatility can be obtained simultaneously over the cerebral vasculature.[16, 17]

Here, we investigate longitudinal relationships (lead–lag and change-change) between 4D flow MRI measures of cerebral arterial pulsatility, WML volume and PVS volume across 5 years, as well as lacune status at baseline, in a population-based cohort followed over the years where cerebrovascular changes typically debut.

Materials and Methods

Participants

The current study analyzed data from a sub-cohort of the Cognition, Brain, and Aging (COBRA) study.[19] Participants were randomly selected from the population registry in Umeå, Sweden. The study was conducted in accordance with the Declaration of Helsinki and approved by the Regional Ethical board of Umeå, Sweden. Written informed consent was provided from all participants prior to any testing.

COBRA is a prospective aging study for which healthy individuals (n = 181; Mini-Mental State Examination [MMSE] score ≥ 27) in the ages 64–68 years underwent baseline assessments of brain, cognition, health, and lifestyle during 2012–2014.[19] Out of these, 70% returned for a 5-year follow up (n = 129). Exclusion criteria at baseline included traumatic brain injury, symptomatic stroke, dementia, intellectual disability, epilepsy, psychiatric and neurological disorders, diabetes, certain medications that can alter cognitive performance, severe visual or auditory impairment, claustrophobia, and poor Swedish language skills.

The MRI images were evaluated by a neuroradiologist for presence of structural abnormalities (tumors, hemorrhages, signs of strokes). Hypertension status (including the prescription of antihypertensive agents) was determined from clinical routine examinations only. Table 1 shows observed data at baseline.

TABLE 1. Descriptive statistics of the observed data

	Full sample	Returnees	Dropouts	Selectivity	$r_{T1 \, vs. \, T2}$
ICA PI	0.98 (0.14)	0.97 (0.12)	1.00 (0.16)	−0.07	0.60[a]
Distal PI	0.87 (0.10)	0.87 (0.10)	0.87 (0.11)	0.00	0.56[a]
WML vol (mL)	2.46 (2.41)	2.16 (2.14)	3.09 (2.81)[a]	−0.13	0.94[a]
PVS vol (mL)	11.7 (6.01)	11.6 (6.41)	11.7 (5.30)	−0.01	0.81[a]
Lacunes	29%	25%	42%[a]	−0.11	0.90[a]
Hypertension	33%	30%	42%	−0.07	0.46[a]
SBP (mmHg)	142 (17.4)	141 (16.1)	144 (20.0)	−0.05	0.47[a]

Note: Vascular indicators at baseline are compared between returnees and dropouts and in relation to the parent sample (selectivity), and between baseline and follow-up for the returnee sample using correlation ($r_{T1 \, vs. \, T2}$).
[a]Indicates $p < 0.05$ for comparisons between returnees and dropouts at baseline (using independent samples t-tests or fisher's exact tests) and for $r_{T1 \, vs. \, T2}$ (using Pearson correlation). Lacune positive indicates at least one lacunar infarct present on MRI. Selectivity represents the mean value for returnees at baseline, standardized to the mean value and standard deviation for the parent sample at baseline. PI, pulsatility index; PVS, total perivascular space volume in basal ganglia, white matter, and brainstem; SBP, systolic blood pressure; WML, whole-brain white matter lesion volume.

Magnetic Resonance Imaging

MRI acquisitions were done using a 3 T scanner (Discovery MR 750; GE Healthcare, Milwaukee, Wisconsin) with a 32-channel head coil. These included 4D flow MRI for cerebral arterial pulsatility, and structural MRI, including T_1-weighted, T_2-weighted and fluid attenuated inversion recovery (FLAIR) for segmentation of WML (T_1 & FLAIR) and PVS (T_1 & T_2) volumes. None of the scans were done with any contrast media.

4D Flow MRI. The 4D flow scans were acquired with a PC-VIPR (Phase Contrast Vastly undersampled Isotropic-voxel Projection Reconstruction) sequence that provides flow velocities in all spatial directions, time-resolved over the cardiac cycle, and with whole-brain coverage.[11] The PC-VIPR sequence utilizes radial sampling of k-space, making it less sensitive to motion and pulsatile artifacts.[11] Imaging parameters: 5-point velocity encoding (venc): 110 cm/s, TR/TE: 6.5/2.7 ms, flip angle: 8 °, radial projections: 16000, temporal resolution: 20 frames per cardiac cycle, matrix size at acquisition: 300x300x300, imaging volume: $22 \times 22 \times 22$ cm^3, matrix size after reconstruction: $320 \times 320 \times 320$, spatial resolution: 0.69 mm isotropic. Scan time was approximately 9 min. Velocity data (x, y, z, t) and a complex difference (CD) volume used to highlight vascular structure were reconstructed from the 4D flow scans.

Structural MRI. The T_1-weighted scans were done with a 3D fast-spoiled gradient echo sequence acquired with the following parameters: TR/TE: 8.2/3.2 ms, flip angle: 12 °, number of slices: 176, slice thickness: 1 mm, in-plane resolution: 0.94 mm, and field of view: 25×25 cm, and phase acceleration: 2. The T_2-weighted scans were acquired with an axial fast relaxation fast spin echo (FRFSE) sequence using the following parameters: TR/TE: 7576/100 ms, auto refocused flip angle: 111 °, number of slices: 48, slice thickness: 3 mm, in-plane resolution: 0.5×0.9 mm, field of view: 24×24 cm, and phase acceleration: 2. FLAIR scans were acquired with the following parameters: TR/TE: 8000/120 ms, slice thickness: 3 mm, number of slices: 46, in-plane resolution: 0.94 mm, and field of view: 24×24 cm.

4D Flow MRI Waveform Extraction

All 4D flow MRI data were processed using MATLAB (Natick, Massachusetts: The MathWorks Inc). Pulsatile flow waveforms were sampled for the internal carotid arteries (ICA) and for small, distal cerebral arteries using inhouse-developed semi-
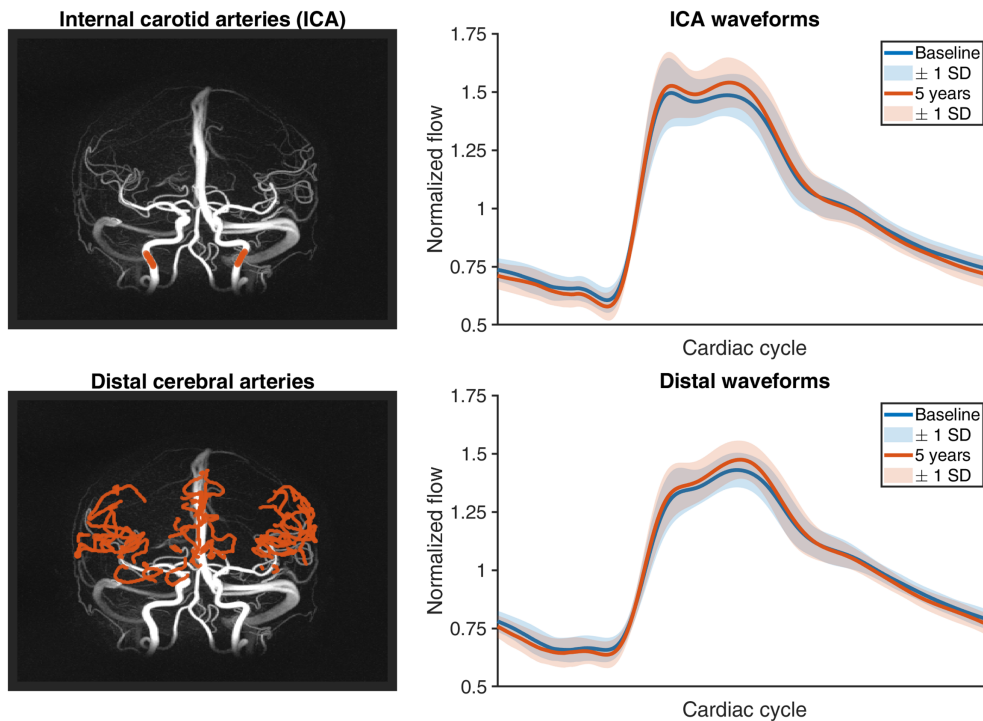
FIGURE 1: The 4D flow MRI complex difference angiograms and waveforms. The left panels display vessels for an example subject at baseline, where the red color corresponds to the identified vessel cross-sections used to estimate the internal carotid artery (ICA) and the distal arterial waveform. On a subject level, the ICA waveform corresponds to the average of the left and right ICAs, and the distal waveform corresponds to the median waveform of all identified distal cross-sections. The individual waveforms were interpolated from 20 to 2000 frames and synchronized after the systolic onset before pulsatility index (PI) calculation. The right panels display subject-averaged waveforms at baseline and 5-year follow-up for the entire sample, with transparent bounds representing ± 1 standard deviation (SD).

automatic post-processing methods.[13, 14, 17] A visualization of identified large (ICA) and small (distal) cerebral arteries for an example participant, as well as corresponding group-averaged flow waveforms at baseline and follow-up, is provided in Fig 1.

The ICA measurements were performed in the extracranial ICA at the cervical (sometimes reaching the petrous) segment, by visual inspection of the CD volume and manually placed seed points (Fig 1). Waveforms were then calculated from these seed points using a semi-automatic post-processing approach.[13] Briefly, a centerline structure was obtained from the CD volume using intensity-based thresholding and pruning of the binary vascular tree. Then, orthogonal planes were automatically placed along the centerline branch near the seed points and a local threshold (20% of the CD local maximum intensity) was used to identify the vessel segment from stationary tissue.[14] Finally, time-resolved 4D flow velocity data were sampled and spatially averaged along 15 neighboring cross-sections originating from the same vessel branch. Hence, each ICA branch is represented by a single pulsatile waveform obtained by averaging data from 15 adjacent cross-sections. The left and right ICA waveforms are then averaged into a single ICA waveform before pulsatility analysis.

Distal cerebral arteries, corresponding mainly to distal branches of the anterior, middle, and posterior cerebral arteries, were identified using a previously evaluated automatic post-processing method utilizing vessel size and waveform information to exclude large arteries and veins.[17] First, a vessel enhancement filter was applied to the CD volume to boost visualization of small vessels.[20] A centerline structure was then obtained using intensity-based thresholding of the filtered CD volume and pruning of the binary vascular tree.[13] Next, planes were automatically placed along the centerline structure of the entire cerebral vascular tree, and a local threshold was used to identify small vessels from stationary tissue and noise. Distal cerebral arteries were identified using a combination of waveform-clustering to separate arteries and veins, a binary mask to exclude extracranial vessels, and a diameter threshold to exclude vessels with a diameter estimate >1.25 mm. The distal arterial tree was then inspected and pruned to remove accidentally included veins and extracranial arteries. Finally, the flow data from all identified distal cerebral arterial cross-sections (1,494 ± 574 at baseline; 1,387 ± 574 at follow-up) were normalized and combined into a composite flow waveform. Hence, the distal arterial waveform is a global representation of pulsatile hemodynamics in small cerebral arteries.[17]

Waveform Analysis

The final ICA and distal waveforms were characterized by the PI:

$$PI = \frac{\max(Q) - \min(Q)}{\text{mean}(Q)},$$

where Q is the flow waveform obtained after averaging waveforms from the identified cross-sections. Hence, ICA and distal PIs were estimated once per individual. Before calculating the PI, the temporal resolution of the waveforms was increased from 20 to 2000 frames per cardiac cycle using cubic splines interpolation. This was done to be consistent with previous pulsatility analyses at baseline, where interpolation was necessary to allow for synchronization with respect to the cardiac cycle.[16]

WML Segmentation

SPM12 and a lesion-growth algorithm[21] implemented in the LST toolbox was used to segment total WML volume, using T_1-weighted and FLAIR volumes as input. The T_1-weighted volume was used to estimate tissue probability maps for gray matter, white matter, and cerebrospinal fluid. The FLAIR volume was, in combination with the tissue probability maps, used to create a lesion probability map using a pre-defined threshold ($\kappa = 0.3$) and region growing. Finally, total WML volume was obtained from the lesion probability map using a 50% threshold. The segmented volumes were evaluated against visually determined deep (Spearman's $\rho = 0.62$, $p < 0.001$) and periventricular (Spearman's $\rho = 0.64$, $p < 0.001$) Fazekas scores.

PVS Segmentation

PVSs were segmented with an in-house algorithm implemented in MATLAB, inspired by previous methods using T_1- and T_2-weighted volumes as well as morphological information to identify PVSs.[22, 23] First, our T_1 and T_2-weighted volumes were resampled to an isotropic resolution of 1 mm and spatially co-registered to obtain a quotient volume defined as the T_2 / T_1 ratio computed for each voxel, where a dilated PVS would display high intensities. To further boost PVS visualization, a filter used to enhance vascular morphology was applied to the quotient volume.[20] The filtered volume was then thresholded to obtain segments. In addition, tissue probability maps obtained from the T_1-weighted volumes were used to confine the segmentations to gray- and white-matter only. This mask was slightly eroded (3 voxels) to avoid false PVS identification near the edges of a region. Total PVS volume used for statistical analyses was obtained by combining PVS volumes in basal ganglia, white matter, and brainstem. The segmented PVS volumes were evaluated against a visual rating scale[24] (Table 2).

Lacunar Infarcts

The presence of lacunar infarcts was determined by visual inspection according to the STRIVE recommendations.[25] Lacunes were defined as small (3–15 mm) subcortical fluid-filled lesions, appearing as hyperintensities on T_2-weighted volumes and hypointensities on T_1-weighted and FLAIR volumes. An additional feature utilized for differentiation from PVSs was increased FLAIR signal in the rim of lacunes.

Statistics

Two types of models were used for statistical analyses: linear mixed effects (LMEs) models and latent change score (LCS) models. LME models were used to investigate the effect of time on each vascular outcome and to explore change-change and change-level associations. LCS models, that belong to a class of structural equation models, were then used to model such relationships among the vascular outcomes simultaneously, thus

TABLE 2. Perivascular spaces (PVS) by visual inspection of the semioval center, and by automatic segmentation in cerebral white matter

Baseline				
Visual scale	1	2	3	4
N	20	47	90	21
Volume (mL)	2.41 (0.25)	4.70 (0.32)	9.82 (0.38)	15.15 (1.06)
Follow-up				
Visual scale	1	2	3	4
N	5	15	56	38
Volume (mL)	2.65 (0.23)	5.5 (0.64)	9.85 (0.52)	19.14 (0.86)

Note: Visual scale according to Potter et al.[24] Volumes indicate mean ± 1 SE for each corresponding subsample. The PVS volumes and visual ratings correlated at wave 1 ($r = 0.79$; $p < 0.001$) and wave 2 ($r = 0.80$; $p < 0.001$).

refining the focus on change and time-lagged associations between vascular outcomes.[26, 27] Both models were adjusted for baseline age and time-varying hypertension status.

LME Models. Longitudinal 5-year changes were modeled using LMEs in R with the *nlme* package (version 3.1) as:

$$Y_{i,j} = \beta_0 + \beta_1 Time_{i,j} + \beta_2 Age_j + \beta_3 HT_{i,j} + \mu_{0,j} + \mu_{1,j} Time_{i,j} + \epsilon_{i,j}, \quad (1)$$

where $Y_{i,j}$ denotes the modeled variable (e.g., PI, WML volume, or PVS volume), $Time_{i,j}$ denotes the time point (0 or 5 years) at time i for individual j, Age_j denotes the mean-centered baseline age for individual j, and $HT_{i,j}$ denotes hypertension status at time i for individual j. The fixed effects are described by β_0, β_1, β_2 and β_3, whereas $\mu_{0,j}$ and $\mu_{1,j}$ denotes the random intercepts and slopes, respectively. The participant-specific intercepts (I_j) and slopes (δ_j) are then estimated as $I_j = \beta_0 + \mu_{0,j}$ and $\delta_j = \beta_1 + \mu_{1,j}$.

The p-values describing significant age-related changes were based on the LME fixed effects. The Pearson's correlation coefficient (r) was determined for participant-specific intercept – intercept ($I - I$), slope – slope ($\delta - \delta$), and intercept – slope ($I - \delta$) associations. Independent samples t-tests were used to evaluate group differences between lacune-positive and lacune-negative individuals. Residualization by regression was used to control WML slopes for WML intercepts when evaluating lacunes in relation to WML progression.

Structural Equation Modeling. The software Onyx (https://onyx-sem.com/) and the R-package Lavaan (version 0.6–9) were used for all structural equation modeling.

The observed data were standardized using z-scores (mean 0; variance 1) and adjusted for age and hypertension through residualization with regression. Before defining the LCS models, confirmatory factor analysis (CFA) was performed to test whether our biomarkers could be combined into a longitudinal SVD score, with ICA PI, distal PI, WML, and PVS as input. In addition, CFAs were performed separately in two simpler models: one with WML and PVS as input, and one with ICA PI and distal PI as input. Acceptable model fit was deemed by root-mean-square error of approximation (RMSEA) < 0.08, comparative fix index (CFI) > 0.90, and standardized root mean residual (SRMR) < 0.08.

Attrition. Independent samples t-test and Fisher's exact test were used to evaluate group differences between drop-out and returnees for pulsatility, WML and PVS volumes, and for lacune and hypertension status (positive/negative). Dropouts and returnees differed in lacune status and WML burden (Table 1). Selectivity was reported to describe group differences between returnees and the full parent sample at baseline (Table 1).

Missing and Excluded Data. Time-resolved 4D flow MRI data were missing for 22 participants at baseline and for 7 participants at follow-up, limiting the pulsatility data to 159 persons at baseline and 122 persons at follow-up, with 108 complete cases. Furthermore, all the pulsatility, WML, and PVS variables were screened for statistical outliers before LME and LCS modeling. Observed data were considered statistical outliers if deviating more than 3.29 standard deviations (SDs) from the mean.[28] This led to the exclusion of one participant for distal PI and two participants for ICA PI at baseline, and to the exclusion of

three participants for WML at baseline and four participants for WML at follow-up. The final samples sizes (at baseline and follow-up) were ICA PI (n = 157/122), distal PI (n = 158/122), WML volume (n = 173/121), PVS volume (n = 178/114), and lacunar infarcts (n = 181/126). Full information maximum likelihood (FIML) was used for incomplete cases in LME and LCS models.

Results

5-Year Longitudinal Changes in Pulsatility and Vascular Lesions

In line with previous longitudinal studies, significant 5-year increases were found for PI[10] and WML volume[29] using LME models (Table 3). We also found a longitudinal expansion of PVS (Table 3), extending cross-sectional age-assocations.[30] Moreover, distal PI and ICA PI were correlated in terms of intercepts (r = 0.80; $p < 0.001$), but also in terms of slopes (r = 0.55; $p < 0.001$), which is a novel longitudinal observation suggesting relatively synchronized age-related pulsatility-increases across the brain.

Longitudinal Associations between Pulsatility and Vascular Lesions

WML and PVS volumes correlated in terms of intercepts (r = 0.37, $p < 0.001$), but not slopes (r = 0.01, $p = 0.89$). Moreover, while WML intercept was unrelated to PVS slope (r = 0.04, $p = 0.71$), PVS intercept was related to WML slope (r = 0.34, $p < 0.001$), agreeing with previous studies.[31, 32] Furthermore, PI was unrelated to WML and PVS volumes at baseline, and neither ICA or distal PI predicted WML or PVS progression (Table 4). However, larger distal PI increases were related to more rapid WML progression, and higher WML and PVS volumes at baseline were related to larger ICA and distal PI increases across 5 years (Table 4). Collectively,

these are novel longitudinal observations suggesting that pulsatility and vascular lesions are related in a lead–lag fashion, where structural SVD manifestations predict PI increases over time.

Next, CFA was performed to further assess whether biomarkers are interrelated, and suitable as indicators of one overall latent factor of SVD. The CFAs showed poor model fit when combining all four biomarkers (ICA PI, distal PI, WML, and PVS) into a latent factor (RMSEA ≥ 0.27; CFI ≤ 0.45; SRMR ≥ 0.25), and when combining WML and PVS into a latent factor (RMSEA ≥ 0.34; CFI ≤ 0.76; SRMR ≥ 0.17), independent of parameter constraints. Hence, although PI, WML, and PVS are features of SVD, they do not coalesce into a single SVD score, a finding suggesting they reflect non-overlapping brain properties. Nevertheless, combining ICA PI and distal PI into a latent PI showed excellent model fit (RMSEA < 0.001; CFI > 0.999; SRMR < 0.001) when constraining loadings, means, and variances across time points, with similar loadings for ICA PI (1.00) and distal PI (0.93), and significant variance in change ($\sigma^2 = 0.40$; $p < 0.001$). These results demonstrate that (1) ICA and distal PI are highly correlated, indicating they could be combined into one latent PI measure, and (2) there are large individual differences in change for PI in aging.

Finally, we applied a latent change score (LCS) framework that is specifically designed to investigate longitudinal relationships, including age-lagged changes, by modeling several relationships among variables simultaneously.[26] Since the CFAs only showed acceptable fit for the latent PI model, we defined three bivariate LCS models[27] (Fig 2) and evaluated the longitudinal associations between the latent PI factor in relation to WML volume (Fig 2A) and PVS volume (Fig 2B) separately, and then WMLs in relation PVSs (Fig 2C). In line with our previous results from LMEs (Table 4), the LCS models supported that 5-year pulsatility increases were predicted

---

TABLE 3. LME model fixed effects

	Intercept age 65	5-year change	*p*-value change
ICA PI	0.98 (0.95, 0.98)	0.06 (0.03, 0.08)	**<0.001**
Distal PI	0.87 (0.84, 0.90)	0.05 (0.03, 0.07)	**<0.001**
WML vol. (mL)	2.39 (1.90, 2.87)	1.33 (1.04, 1.63)	**<0.001**
PVS vol. (mL)	11.6 (9.93, 13.4)	4.51 (3.57, 5.45)	**<0.001**

Note: Intercept at age 65 and 5-year change as estimated from the LME model fixed effects, with brackets denoting 95% confidence intervals. *p*-values correspond to the 5-year change fixed effects. All models are adjusted for baseline age and hypertension. ICA, internal carotid artery; LME, linear-mixed effects; PI, pulsatility index; PVS, total perivascular space volume in basal ganglia, white matter, and brainstem; WML, whole-brain white matter lesion volume.

TABLE 4. Pulsatility in relation to WML and PVS based on LME models random effects

	WML intercept	PVS intercept	WML slope	PVS slope
ICA PI intercept	R = 0.11; p = 0.29	R = 0.16; p = 0.13	R = 0.11; p = 0.23	R = -0.03; p = 0.78
Distal PI intercept	R = 0.03; p = 0.75	R = 0.10; p = 0.32	R = 0.02; p = 0.86	R = -0.12; p = 0.26
ICA PI slope	R = 0.25; **p = 0.014**	R = 0.23; **p = 0.025**	R = 0.19; p = 0.067	R = 0.11; p = 0.28
Distal PI slope	R = 0.24; **p = 0.015**	R = 0.32; **p = 0.002**	R = 0.26; **p = 0.009**	R = 0.15; p = 0.15

Note: Intercept and slope denotes participant-specific intercepts and slopes obtained from the LME models random effects. Correlation coefficients (R) and p-values are obtained from Pearson correlation. ICA, internal carotid artery; LME, linear-mixed effects; PI, pulsatility index; PVS, perivascular space; WML, white matter lesion.
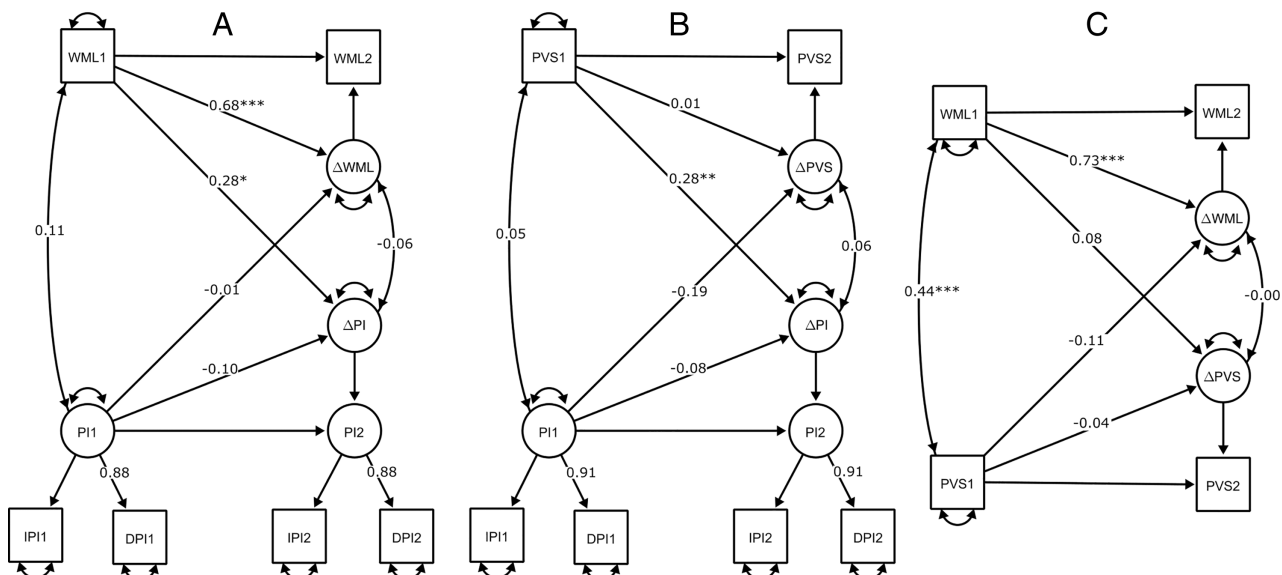

FIGURE 2: Associations among vascular biomarkers over 5 years of aging. (a-b) Latent change score (LCS) models evaluating pulsatility in relation to (A) white matter lesion (WML) volume and (b) perivascular space (PVS) volume, with a latent pulsatility index (PI) constructed from ICA PI (IPI) and distal arterial PI (DPI). Baseline WML and PVS volumes were both predictive of 5-year increments in pulsatility, as shown for (a) WML volume ($\beta = 0.28$; $p = 0.015$) and (b) PVS volume ($\beta = 0.28$; $p = 0.009$). No baseline or change-change associations were found for PI in relation to WML or PVS volumes. (c) LCS model evaluating WML volume in relation to PVS volume, indicating a high correlation at baseline (r = 0.44; $p < 0.001$), with no baseline-change or change-change associations between WML and PVS. Note: The reported regression and covariance coefficients reflect standardized estimates. All model fits were deemed acceptable (RMSEA < 0.05; CFI >0.99; SRMR<0.03).

by baseline burden of WML ($\beta = 0.28$; $p = 0.015$) and PVS ($\beta = 0.28$; $p = 0.009$) volumes (Fig 2A,B). However, there was no change-change association between pulsatility and WML in the LCS model (Fig 2A). Furthermore, consistent with the LME results (Table 4), pulsatility was unrelated to WML and PVS volumes at baseline and did not predict WML and PVS progression across 5 years (Fig 2A,B).

The LCS framework also supported a link between WML and PVS volumes at baseline; however, the link between baseline PVS volume and WML volume change (Table 4) was completely suppressed in the LCS model (Fig 2C). Conceivably, this reflects that this association was related to WML burden at baseline, as suggested by

the strong correlation between baseline WML volume and WML volume change (Fig 2C).

Effect of Lacunar Infarcts

Among lacune-positive individuals, most had only one lacunar infarct present. Moreover, few individuals (n = 5) went from lacune-negative to lacune-positive over 5 years, limiting the analysis to lacune status at baseline. Lacune-positive individuals had larger WML volume intercepts and slopes, whereas no differences were found for PVS volume or pulsatility (Table 5). However, when controlling WML slopes for WML intercept, no differences were found between lacune-positive and lacune-negative individuals (Table 5).

TABLE 5. Differences in PI, WML volume (mL), and PVS volume between lacune positive (at least one lacune present on MRI) and lacune negative individuals

	Lacune status		
	Not present	Present	*p*-value (ind. t-test)
ICA PI intercept	0.98 ± 0.10 (0.96, 1.00)	0.99 ± 0.11 (0.95, 1.04)	0.54
ICA PI slope	0.05 ± 0.09 (0.03, 0.07)	0.07 ± 0.07 (0.04, 0.10)	0.28
Distal PI intercept	0.87 ± 0.08 (0.85, 0.89)	0.87 ± 0.08 (0.84, 0.90)	0.73
Distal PI slope	0.04 ± 0.07 (0.03, 0.06)	0.05 ± 0.06 (0.03, 0.08)	0.50
WML intercept	2.06 ± 1.80 (1.69, 2.44)	3.53 ± 2.38 (2.57, 4.49)	**0.006**
WML slope	1.14 ± 1.24 (0.88, 1.40)	2.01 ± 1.34 (1.47, 2.55)	**0.005**
Adj. WML slope[a]	0.01 ± 0.51 (−0.11, 0.13)	0.12 ± 0.59 (−0.11, 0.34)	0.41
PVS intercept	11.2 ± 5.52 (10.0, 12.4)	12.9 ± 6.49 (10.4, 15.4)	0.23
PVS slope	4.55 ± 3.02 (3.39, 5.20)	4.40 ± 2.72 (3.35, 5.45)	0.81

Note: intercept and slope denote participant-specific intercepts and slopes obtained from linear mixed-effects models. Intercepts and slopes are adjusted for baseline age and hypertension. ICA, internal carotid artery; PI, pulsatility index; PVS, perivascular space; WML, white matter lesion.
[a]Further adjusted for WML intercept by regression.

Discussion

We evaluated 5-year changes in cerebral arterial pulsatility, WML volume, and PVS volume, in a population-based cohort of healthy older adults. Our main findings were that, although pulsatility at baseline did not predict WML and PVS progression, more WML and PVS volume at baseline were related to larger increases in cerebral arterial pulsatility across 5 years. These time-lagged associations do not support pulsatility as an early contributing mechanism in cerebral SVD. Instead, our findings suggest that individuals with higher WML and PVS burden at baseline are prone to exhibit larger PI increases over time. We interpret this as a cascade of events where subtle microvascular damage underlying WML and PVS progression also leads cerebral arterial PI increases over time, potentially due to the sensitivity of PI to downstream microvascular resistance. These findings align with a recent study where PI at baseline failed to predict WML progression over 5 years.[10] Importantly, our study extends previous studies[9, 10] from merely testing whether baseline pulsatility predicts WML progression, by also testing the alternative hypothesis that those with larger WML and PVS volumes at baseline are more prone to demonstrate increased PI over time. Furthermore, this is the first longitudinal study on pulsatility and PVS dilation. As such, the current work provides novel insights on the dynamics among these vascular indicators in aging.

The PI of both ICA and distal cerebral arteries was estimated to increase with approximately 1% per year, which agrees with our previous cross-sectional observations.[17]

Furthermore, ICA and distal PI were highly correlated at baseline, with strong change-change associations, but no baseline-change relations. In addition, the latent PI construct showed excellent model fit. These results are not surprising, considering that both ICA and distal PI largely correspond to a global representation of the cerebral arterial waveform, although the distal measurements are performed further out in the vasculature. However, focal measurements in regions of particular interest could be advantageous in future SVD studies. Indeed, 2D phase contrast MRI at 7T allows for pulsatility[33] and damping[34] measurements in perforating arteries of the basal ganglia and semioval center, regions of particular interest in SVD. This approach showed higher pulsatility in patients with SVD-related stroke.[35] That said, our findings demonstrate that 4D flow MRI, with a scan time of less than 10 minutes, is sensitive enough for detecting 5-year changes in both large and small cerebral arteries and relate them to structural features of SVD.

Although WML and PVS volumes were related at baseline, no change-change associations were found. Furthermore, our attempts to construct a latent SVD score in longitudinal SVD models failed, potentially due to limited shared variance in change among the observed variables. Thus, although these markers are considered manifestations of SVD, changes in them were not coupled over a period of 5 years in a relatively healthy sample aged 64 to 68 years at baseline. These findings may reflect that PVSs and WMLs appear at different times and stages in SVD. Indeed, some evidence suggests that WMLs tend to form around PVSs[3]. In addition, the omission

of microbleeds and lacunes may have hampered the ability to establish a latent SVD variable. Notably, a cross-sectional study constructed a latent SVD score by integrating WML volume, PVS volume, lacunes, and microbleeds, indicating shared variance.[36] This underlines the discrepancies that can arise when interpreting patterns from between-person versus within-person assessments and accentuates the need of future longitudinal studies that depict changes in several biomarkers from middle adulthood to advanced old age.

We used two statistical approaches for longitudinal data analysis, LME and LCS models. The LME models were used to describe age-related changes and to evaluate pairwise associations, whereas the LCS framework allowed us to model associations among several variables simultaneously.[27] Interestingly, our LME findings indicated that lacunes and PVS at baseline predicted WML change. The PVS finding aligns with suggestions that PVS dilation could be a pre-stage to WML progression[32]; however, in line with another study,[31] the link between baseline PVS and WML change was suppressed in the LCS model. Moreover, our link between lacunes at baseline and WML slopes vanished when controlling for WML intercepts. Hence, these associations were both dependent on WML burden at baseline. This highlights the benefits of modeling multiple longitudinal relationships simultaneously. Importantly, our main finding, namely that WML and PVS volumes predicted 5-year increases in cerebral arterial PI, was obtained with either model. Furthermore, PI and WML outliers were excluded when deviating 3.29 SD from the mean. However, all analyses were repeated without outlier exclusion (not reported here), with similar results for all main analyses, with the only distinction that dropouts and returnees did not differ in WML burden at baseline (Table 1) when including the outliers.

Our findings do not rule out excessive vascular pulsatility as a mechanism harmful to the cerebral microcirculation.[6] Vascular aging is associated with aortic stiffness, elevated pulse pressure, and compromised cerebral arterial damping-capacity – factors that in turn facilitate transmission of cardiac-generated pulsatility to the cerebral microcirculation.[37, 38] However, periventricular white matter is supplied by long arteries that branch into tortuous arterioles,[39] potentially limiting the transfer of hemodynamic stress.[40] Instead, brain regions with a vascular supply characterized by short arterial branches that provide little damping-capacity could be particularly susceptible to pulsatile stress, potentially explaining why pulsatility correlates negatively with hippocampal volume[41, 42] and episodic memory.[16] Importantly, BBB breakdown begins in the hippocampus and accelerates cognitive decline.[43] Hence, pulsatility may be particularly interesting to study in relation to hippocampal BBB breakdown. In other

longitudinal studies, aortic pulse wave velocity (PWV) has been shown to predict WML progression[44] and incident microbleeds.[45] Considering the results of the present study, this indicates that central PWV and cerebral arterial PI progress differently in the course of aging and SVD. This underscores that PWV and PI partially reflect different properties of the vascular system, with PWV more specifically relating to vascular stiffness, whereas PI display additional sensitivity to microvascular resistance.

PVSs are cerebrospinal-fluid filled cavities that surround penetrating vessels, and may function as fluid transport passages in the glymphatic system for clearance of metabolic waste.[3] However, whether PVS dilation is harmful, or whether it is an epiphenomenon, is debated.[3] In contrast to PVSs, there is compelling evidence that lacunar infarcts[46] and large (confluent) WMLs[1] are harmful to the brain. However, although lacunes, WMLs, and dilated PVSs are distinct manifestations of microvascular damage, they may still share an underlying etiology. Indeed, BBB breakdown on a brain-wide level could be involved in the pathogenesis of PVS dilation,[3] lacunar infarcts[46] and WML progression.[47] Hence, future longitudinal studies should consider BBB permeability imaging in relation to biomarker progression over time.

There are a few limitations concerning the structural SVD biomarkers. Few individuals (n = 5) changed from lacune-negative to lacune-positive at follow-up. Hence, we chose not to analyze change in lacune status in relation to pulsatility and the other imaging biomarkers. In addition, dropouts were more severely affected by WMLs and lacunes than returnees. However, the FIML approach utilized by LME and LCS models is resilient against dropout bias. Moreover, the average WML and PVS volumes were relatively small (Tables 1 and 2). A low disease burden impacts power, constraining the ability to detect weaker associations among the investigated variables. This partially reflects that our sample is relatively healthy, as individuals with symptomatic stroke or an MMSE score of less than 27 were excluded. Hence, it is difficult to extrapolate the results from our population to older subjects, or patients with more severe SVD, such as lacunar ischemic stroke syndromes or CADASIL. Importantly, although additional longitudinal data are needed to verify these associations, our findings highlight that WMLs and pulsatility are related over time in a healthy older population. Furthermore, we used an inhouse-developed method for automatic PVS segmentation, with an average total PVS estimate (basal ganglia, white matter, and brainstem) of 11.7 mL and 16.2 mL at baseline and follow-up, respectively. The absolute values of these volumes should however be treated with caution, as they may differ between methods. For instance, Boespflug et al.[22] found a

mean total PVS volume of approximately 0.3 mL among older adults (mean age 85), whereas Barisano et al.[48] reported an average white-matter PVS volume in of 5 mL in young individuals (mean age 29). Further, Cai et al.[49] found a relative PVS volume corresponding to 4.9% of white matter volume in healthy controls (mean age of 69), corresponding to approximately 20 mL assuming a white matter volume of 400 mL. These pronounced PVS volume differences underscores the importance of establishing methodological standards.[50] Toward this end, our method demonstrated agreement with a visual PVS scale (Table 2) and pronounced age-related increases in PVS volume (Table 3).

In conclusion, our observations suggest that in healthy older adults from the population, structural and hemodynamic features commonly associated with SVD are longitudinally related in a lead–lag fashion, in which the expressions of WML and PVS precede increases in cerebral arterial pulsatility. Moreover, lacunes and PVS at baseline were related to WML progression over time, but these associations were dependent on WML burden at baseline. Collectively, our findings suggests that individuals with high WML and PVS burden are prone to exhibit larger cerebral arterial PI increases over time. Hence, we propose that elevated pulsatility is a relatively late manifestation, rather than a risk factor, for cerebral SVD.

Author Contributions

T.V., N.K., U.L., K.R., L.B., LN., and A.W. contributed to conception and design of the study; all authors contributed to acquisition and analysis of data; T.V. and A.W. contributed to drafting and preparing the figures.

Potential Conflicts of Interest

Nothing to report.

References

1. Wardlaw JM, Smith C, Dichgans M. Small vessel disease: mechanisms and clinical implications. Lancet Neurol 2019;18:684–696.

2. Debette S, Schilling S, Duperron M-G, et al. Clinical significance of magnetic resonance imaging markers of vascular brain injury: a systematic review and meta-analysis. JAMA Neurol 2019;76:81–94.

3. Wardlaw JM, Benveniste H, Nedergaard M, et al. Perivascular spaces in the brain: anatomy, physiology and pathology. Nat Rev Neurol 2020;16:137–153.

4. Das AS, Regenhardt RW, Vernooij MW, et al. Asymptomatic cerebral small vessel disease: insights from population-based studies. J Stroke 2019;21:121–138.

5. Shi Y, Thrippleton MJ, Marshall I, Wardlaw JM. Intracranial pulsatility in patients with cerebral small vessel disease: a systematic review. Clin Sci (Lond) 2018;132:157–171.

6. Wåhlin A, Nyberg L. At the heart of cognitive functioning in aging. Trends Cogn Sci 2019;23:717–720.

7. De Montgolfier O, Pinçon A, Pouliot P, et al. High systolic blood pressure induces cerebral microvascular endothelial dysfunction, neurovascular unit damage, and cognitive decline in mice. Hypertension 2019;73:217–228.

8. Garcia-Polite F, Martorell J, Del Rey-Puech P, et al. Pulsatility and high shear stress deteriorate barrier phenotype in brain microvascular endothelium. J Cereb Blood Flow Metab 2017;37:2614–2625.

9. Lee W-J, Jung K-H, Ryu YJ, et al. Progression of cerebral white matter hyperintensities and the associated sonographic index. Radiology 2017;284:824–833.

10. Kneihsl M, Hofer E, Enzinger C, et al. Intracranial pulsatility in relation to severity and progression of cerebral white matter hyperintensities. Stroke 2020;51:3302–3309.

11. Gu T, Korosec FR, Block WF, et al. PC VIPR: a high-speed 3D phase-contrast method for flow quantification and high-resolution angiography. AJNR Am J Neuroradiol 2005;26:743–749.

12. Wåhlin A, Eklund A, Malm J. 4D flow MRI hemodynamic biomarkers for cerebrovascular diseases. J Intern Med 2021;291:115–127. https://doi.org/10.1111/joim.13392.

13. Schrauben E, Ambarki K, Spaak E, et al. Fast 4D flow MRI intracranial segmentation and quantification in tortuous arteries. J Magn Reson Imaging 2015;42:1458–1464.

14. Dunås T, Holmgren M, Wåhlin A, et al. Accuracy of blood flow assessment in cerebral arteries with 4D flow MRI: evaluation with three segmentation methods. J Magn Reson Imaging 2019;50:511–518.

15. Rivera-Rivera LA, Cody KA, Eisenmenger L, et al. Assessment of vascular stiffness in the internal carotid artery proximal to the carotid canal in Alzheimer's disease using pulse wave velocity from low rank reconstructed 4D flow MRI. J Cereb Blood Flow Metab 2021;41:298–311.

16. Vikner T, Eklund A, Karalija N, et al. Cerebral arterial pulsatility is linked to hippocampal microvascular function and episodic memory in healthy older adults. J Cereb Blood Flow Metab 2021;41:1778–1790.

17. Vikner T, Nyberg L, Holmgren M, et al. Characterizing pulsatility in distal cerebral arteries using 4D flow MRI. J Cereb Blood Flow Metab 2020;40:2429–2440.

18. Björnfot C, Garpebring A, Qvarlander S, et al. Assessing cerebral arterial pulse wave velocity using 4D flow MRI. J Cereb blood Flow Metab 2021;41:2769–2777.

19. Nevalainen N, Riklund K, Andersson M, et al. COBRA: a prospective multimodal imaging study of dopamine, brain structure and function, and cognition. Brain Res 2015;1612:83–103.

20. Jerman T, Pernus F, Likar B, Spiclin Z. Enhancement of vascular structures in 3D and 2D angiographic images. IEEE Trans Med Imaging 2016;35:2107–2118.

21. Schmidt P, Gaser C, Arsic M, et al. An automated tool for detection of FLAIR-hyperintense white-matter lesions in multiple sclerosis. Neuroimage 2012;59:3774–3783.

22. Boespflug EL, Schwartz DL, Lahna D, et al. MR imaging-based multimodal autoidentification of perivascular spaces (mMAPS): automated morphologic segmentation of enlarged perivascular spaces at clinical field strength. Radiology 2018;286:632–642.

23. Schwartz DL, Boespflug EL, Lahna DL, et al. Autoidentification of perivascular spaces in white matter using clinical field strength T(1) and FLAIR MR imaging. Neuroimage 2019;202:116126.

24. Potter GM, Chappell FM, Morris Z, Wardlaw JM. Cerebral perivascular spaces visible on magnetic resonance imaging: development of a qualitative rating scale and its observer reliability. Cerebrovasc Dis 2015;39:224–231.

25. Wardlaw JM, Smith EE, Biessels GJ, et al. Neuroimaging standards for research into small vessel disease and its contribution to ageing and neurodegeneration. Lancet Neurol 2013;12:822–838.

26. McArdle JJ, Hamgami F, Jones K, et al. Structural modeling of dynamic changes in memory and brain structure using longitudinal data from the normative aging study. J Gerontol, Ser B 2004;59:P294–P304.

27. Kievit RA, Brandmaier AM, Ziegler G, et al. Developmental cognitive neuroscience using latent change score models: a tutorial and applications. Dev Cogn Neurosci 2018;33:99–117.

28. Tabachnick BG, Fidell LS. *Using Multivariate Statistics*. 6th ed., 2012. London: Pearson Education.

29. Schmidt R, Seiler S, Loitfelder M. Longitudinal change of small-vessel disease-related brain abnormalities. J Cereb blood Flow Metab 2016;36:26–39.

30. Francis F, Ballerini L, Wardlaw JM. Perivascular spaces and their associations with risk factors, clinical disorders and neuroimaging features: a systematic review and meta-analysis. Int J Stroke 2019;14:359–371.

31. Loos CMJ, Klarenbeek P, van Oostenbrugge RJ, Staals J. Association between perivascular spaces and progression of white matter Hyperintensities in lacunar stroke patients. PLoS One 2015;10:e0137323.

32. Ding J, Sigurðsson S, Jónsson PV, et al. Large perivascular spaces visible on magnetic resonance imaging, cerebral small vessel disease progression, and risk of dementia: the age, gene/environment susceptibility–Reykjavik study. JAMA Neurol 2017;74:1105–1112.

33. Bouvy WH, Geurts LJ, Kuijf HJ, et al. Assessment of blood flow velocity and pulsatility in cerebral perforating arteries with 7-T quantitative flow MRI. NMR Biomed 2016;29:1295–1304.

34. Arts T, Onkenhout LP, Amier RP, et al. Non-invasive assessment of damping of blood flow velocity Pulsatility in cerebral arteries with MRI. J Magn Reson Imaging 2021;18:1785–1794. https://doi.org/10.1002/jmri.27989.

35. Geurts LJ, Zwanenburg JJM, Klijn CJM, et al. Higher Pulsatility in cerebral perforating arteries in patients with small vessel disease related stroke, a 7T MRI study. Stroke 2019;50:62–68.

36. Staals J, Booth T, Morris Z, et al. Total MRI load of cerebral small vessel disease and cognitive ability in older people. Neurobiol Aging 2015;36:2806–2811.

37. Mitchell GF, Van Buchem MA, Sigurdsson S, et al. Arterial stiffness, pressure and flow pulsatility and brain structure and function: the age, gene/environment susceptibility-Reykjavik study. Brain 2011;134:3398–3407.

38. Zarrinkoob L, Ambarki K, Wahlin A, et al. Aging alters the dampening of pulsatile blood flow in cerebral arteries. J Cereb Blood Flow Metab 2016;36:1519–1527.

39. Akashi T, Takahashi S, Mugikura S, et al. Ischemic white matter lesions associated with medullary arteries: classification of MRI findings based on the anatomic arterial distributions. Am J Roentgenol 2017;209:W160–W168.

40. Spence JD. Blood pressure gradients in the brain: their importance to understanding pathogenesis of cerebral small vessel disease. Brain Sci 2019;9:21. https://doi.org/10.3390/brainsci9020021.

41. Wåhlin A, Ambarki K, Birgander R, et al. Intracranial pulsatility is associated with regional brain volume in elderly individuals. Neurobiol Aging 2014;35:365–372.

42. Miller ML, Ghisletta P, Jacobs BS, et al. Changes in cerebral arterial pulsatility and hippocampal volume: a transcranial doppler ultrasonography study. Neurobiol Aging 2021;108:110–121.

43. Montagne A, Nation DA, Sagare AP, et al. APOE4 leads to blood–brain barrier dysfunction predicting cognitive decline. Nature 2020;581:71–76.

44. King KS, Chen KX, Hulsey KM, et al. White matter hyperintensities: use of aortic arch pulse wave velocity to predict volume independent of other cardiovascular risk factors. Radiology 2013;267:709–717.

45. Ding J, Mitchell GF, Bots ML, et al. Carotid arterial stiffness and risk of incident cerebral microbleeds in older people: the age, gene/environment susceptibility (AGES)-Reykjavik study. Arterioscler Thromb Vasc Biol 2015;35:1889–1895.

46. Wardlaw JM. What causes lacunar stroke? J Neurol Neurosurg Psychiatry 2005;76:617–619.

47. Wardlaw JM, Makin SJ, Valdés Hernández MC, et al. Blood-brain barrier failure as a core mechanism in cerebral small vessel disease and dementia: evidence from a cohort study. Alzheimers Dement 2017;13:634–643.

48. Barisano G, Sheikh-Bahaei N, Law M, et al. Body mass index, time of day and genetics affect perivascular spaces in the white matter. J Cereb Blood Flow Metab 2020;41:1563–1578.

49. Cai K, Tain R, Das S, et al. The feasibility of quantitative MRI of perivascular spaces at 7T. J Neurosci Methods 2015;256:151–156.

50. Smith EE, Biessels GJ, De Guio F, et al. Harmonizing brain magnetic resonance imaging methods for vascular contributions to neurodegeneration. Alzheimer's Dement: Diagn Assess Dis Monit 2019;11:191–204.